An Experimental Investigation of Path Following for an Underwater Snake Robot with a Caudal Fin ⋆

E. Kelasidi * **K. Y. Pettersen** * **A.M. Kohl** * **J. T. Gravdahl** **

* *Centre for Autonomous Marine Operations and Systems, Dept. of Engineering Cybernetics at NTNU, NO-7491 Trondheim, Norway (e-mail: {Eleni.Kelasidi,Kristin.Y.Pettersen, Anna.Kohl@}@itk.ntnu.no).*
** *Dept. of Engineering Cybernetics at NTNU, NO-7491 Trondheim, Norway (e-mail: Tommy.Gravdahl@itk.ntnu.no).*

Abstract:
In this paper, we present a bioinspired underwater snake robot (USR) equipped with a passive caudal (tail) fin. In particular, a highly flexible configuration of a USR is presented, which is capable of locomotion both on ground and underwater due to the robust mechanical and modular designs where additional effectors can be attached at different modules of the robot depending on the requirements of the application. This gives flexibility to the operator, who can thus choose the proper configuration depending on the task to be performed in various uncertain environments on ground and underwater. Experimental results for straight line path following control are obtained for a physical USR, that enable a comparison of the USR motion with and without the passive caudal fin, both for lateral undulation and eel-like motion patterns. The experimental results show that a path following control approach which has previously been proposed for USRs without tail fin, can be directly applied to solve the path following control problem of this bioinspired USR with a passive caudal fin. In particular, it is shown that the path following control approach successfully steers the robot towards and along the desired path, and furthermore the results show that it is possible to almost double the forward velocity of the robot by using a passive caudal fin.

Keywords: Marine Systems, Maritime Robotics, Mechatronics, Intelligent Autonomous Vehicles, Underwater snake robot with passive caudal (tail) fin, LOS path following control.

1. INTRODUCTION

Recently there has been an increasing interest in using bioinspired robotic systems as an alternative to the traditional remotely operated vehicles (ROVs) or autonomous underwater vehicles (AUVs) for underwater applications in the oil and gas industry, biological community, marine archeology etc. In addition, many research groups studying bioinspired robots argue that it is essential to increase the agility and maneuverability of underwater robots. These features are essential for operations at subsea installations and also for operation task in highly uncertain subsea environments (Crespi et al., 2005; Crespi and Ijspeert, 2006; Porez et al., 2014; Stefanini et al., 2012; Sverdrup-Thygeson et al., 2016b,a; Kruusmaa et al., 2014; Kelasidi et al., 2016a). Hence, the robotic community seeks for new solutions suitable for exploration, monitoring, surveillance and maintenance of subsea infrastructures. Swimming snake robots, which are bio-inspired robotic systems that mimic the motion of biological snakes or fish, carry manipulation capabilities as an inherent part of their bodies and can thus be considered good candidates for these types of applications (Kelasidi et al., 2016a).

⋆ Research partly funded by VISTA - a basic research program in collaboration between The Norwegian Academy of Science and Letters, and Statoil, and partly supported by the Research Council of Norway through its Centres of Excellence funding scheme, project no. 223254-NTNU AMOS.

Several bioinspired swimming snake robots have been developed by different research groups (Mclsaac and Ostrowski, 1999; McIsaac and Ostrowski, 2002; Wilbur et al., 2002; Crespi et al., 2005; Crespi and Ijspeert, 2006; Porez et al., 2014; Li et al., 2011; Ye et al., 2004; Yamada et al., 2005; Takayama and Hirose, 2002; Stefanini et al., 2012; Liljebäck et al., 2014; Ayers et al., 2000; Wilbur et al., 2002). Most of the developed swimming snake-like robots are modular multi-articulated robotic systems. However, when it comes to underwater snake robots with additional effectors (tail fin, fins, thrusters), only a few physical systems have been implemented (Porez et al., 2014; Stefanini et al., 2012; Kelasidi et al., 2016b). In Stefanini et al. (2012); Ayers et al. (2000); Wilbur et al. (2002); Porez et al. (2014) the concept of using a tail fin at the last segment, in addition to the joint actuated motion of USRs, is presented. In particular, a new biorobotic platform inspired by the lamprey is developed in project Lampetra (Stefanini et al., 2012). In this concept, at the last segment of the robot a multi-layer fibreglass tail is attached in order to ensure a good fluid dynamic behaviour and propulsion of the robotic platform (Stefanini et al., 2012). A lamprey-inspired robot is implemented based on biomimetic neurotechnology by Knutsen et al. (2004). This robot is functionally a three component system consisting of a rigid hull/electronics bay, a flexible body axis supporting the nitinol actuator, and a thin, passive tail fin. Another swimming robot called AmphiBot III presented in Porez et al. (2014),

consists of eight segments, with the first being the head segment, while in the last segment (tail segment) a caudal fin is attached. A novel concept of an underwater swimming manipulator (USM) with additional thrusters is presented in Sverdrup-Thygeson et al. (2016b,a), while the first developed underwater snake robot that combines the bioinpired USR with a tail thrusters module at the last segment is presented in Kelasidi et al. (2016b). However, the development of more efficient and robust configurations of underwater swimming robots, choosing the proper effectors to increase efficiency with an overall goal to realize operational snake robots for underwater applications, is an open research area.

In this paper we present a new configuration of the underwater snake robot Mamba (Liljebäck et al., 2014; Kelasidi et al., 2016a) where the joint actuated links are combined with a passive caudal fin attached at the last module of the robot. This is an interesting configuration since it has the advantage compared to the configuration with thrusters (Kelasidi et al., 2016b), that it does not produce significant noise, and it will not perturb the surroundings as much as the thrusters, that sometimes beat up silt from the seafloor, something which would decrease the visibility during operations in the subsea environment. These features can be considered essential for several applications in the underwater environment, including archaeological investigation of shipwrecks, and underwater monitoring without disturbing the biological creatures (Kruusmaa et al., 2014). In this paper we investigate whether the passive tail fin brings advantages with respect to the achieved forward velocity compared to using only joint actuation for propulsion. We present experimental results for the two configurations of the robot, with and without a tail fin, which show that compared to the configuration presented in Liljebäck et al. (2014); Kelasidi et al. (2016a), by attaching a passive tail fin the forward velocity is increased by almost 100 %. In particular, the obtained results show that the average forward velocity both for lateral undulation and eel-like motion patterns, is increased to almost the double by using the configuration of the USR with a passive tail fin.

Furthermore, in order to perform the comparative experimental study between a physical robot with and without a passive caudal (tail) fin, we consider the case of path following control. In particular, the paper presents experimental results for a USR with a passive tail fin, using the path following control approach previously proposed and experimentally validated for underwater snake robots without tail fin in Kelasidi et al. (2016a). The experimental results presented in this paper show that the path following control approach can be directly applied to solve the path following control problem of this bioinspired USR with passive caudal tail. In particular, it is shown that the path following control approach successfully steers the robot towards and along the desired path, while at the same time it is possible to almost double the forward velocity.

The paper is organized as follows: Section 2 presents the new configuration of the underwater snake robot Mamba combined with a passive tail fin, while the path following approach is outlined in Section 3. Experimental results for path following of USR Mamba that provides a comparison of its motion with and without a tail fin are presented in Section 4. Finally, Section 5 presents the conclusions of the work, followed by suggestions for further research.

2. UNDERWATER SNAKE ROBOT WITH PASSIVE CAUDAL FIN

Several bioinspired underwater snake-like robots (also referred to as eel-like robots) have been developed by different groups the last decades (Mclsaac and Ostrowski, 1999; McIsaac and Ostrowski, 2002; Wilbur et al., 2002; Crespi et al., 2005; Crespi and Ijspeert, 2006; Porez et al., 2014; Li et al., 2011; Ye et al., 2004; Yamada et al., 2005; Takayama and Hirose, 2002; Stefanini et al., 2012; Liljebäck et al., 2014; Ayers et al., 2000; Wilbur et al., 2002). The underwater snake robot Mamba that is presented briefly in this paper, has been developed at NTNU in Norway. A more detailed description of the robot can be found in Liljebäck et al. (2014); Kelasidi et al. (2016a). The robot is capable of locomotion both on ground and underwater due to the robust mechanical design, where additional effectors (i.e. caudal fin, pectoral fins, thrusters etc.) can be attached at different modules of the robot depending on the requirements of the application. Hence, the robot has a highly flexible and reconfigurable nature that makes it attractive as a testbed for experimental investigation of various configurations of USRs. In Kelasidi et al. (2016b) experimental results for the locomotion efficiency of the USR with and without thrusters are presented. In this paper, we present a configuration where the robot is combined with a passive caudal fin attached at the last segment of the robot.

The underwater snake robot Mamba in this configuration (see Fig. 1) consists of 18 modules that are watertight down to about 5 m, with a common mechanical and electrical interface between the modules, a head module and a passive caudal fin attached at the last module of the robot. A Hitec servo motor (HSR 5990TG) is used for the actuation of each of the 18 joint modules and a microcontroller card (TITechSH2 Tiny Controller from HiBot) is used for the implementation of the necessary low level control of each joint. In addition, each module contains a force/torque sensor, temperature sensors, a 3-axis accelerometer and sensors for water leakage detection. The CAN bus is used for the communication between all the microcontrollers in the modules of the robot, for sending the required reference signal to the robot and for reading the necessary data from the sensors installed inside the modules. Power supply cables (35 V) run through all the modules along with the CAN bus.

The tail fin has a length of 0.5 m and a height of 0.09 m, identical to the height of the modules of the robot. The design of the tail fin in Solidworks, and a photo of the developed tail fin, are shown in Fig. 1a. The tail fin with the strengtheners and the holder are made using Polycarbonate (PC) and Polyvinyl Chloride (PVC), respectively. Note that an opening of 0.12 m on the tail fin, close to the connection point, and additional attachment holders were required for the tether connection. In addition, during the experiments the tail fin was covered with a thin drysuit neoprene material in order to make it neutrally buoyant.

The modules of Mamba are mounted horizontally and vertically in an alternating fashion in order to provide locomotion in 3D plane (Liljebäck et al., 2014). This means that the robot consists of 20 links of length $2l = 0.18$ m and mass $m \approx 0.8$ kg. In this configuration Mamba has a slightly positive buoyancy. In addition, the robot is covered by a watertight skin in order to achieve an additional water barrier as shown in Fig. 1b. Groundsheet, nylon, PU-coated, 120 g/m^2 material and rubber

bottle wrist seals are used for the skin and the sealing of the head and the tail parts, respectively. In order to compare the locomotion efficiency of Mamba with and without the fin, we will use a path following approach which is outlined in Section 3. Note that during the experiments presented in Section 4, the angles of the joints responsible for the vertical motion were set to zero degree in order to constrain the robot to move in a strictly horizontal plane.

3. PATH FOLLOWING

Several control approaches for USRs have been proposed in the literature ((Lapierre and Jouvencel, 2005)(Kelasidi et al., 2016a)(Kelasidi et al., 2017) (McIsaac and Ostrowski, 2003) (Alamir et al., 2007)). A discussion of the different path following approaches proposed for USRs can be found in Kelasidi et al. (2017). In this section, we present briefly the line-of-sight (LOS) path following control approach presented in Kelasidi et al. (2016a) for underwater snake robots. This approach will be applied for the first time for a USR with passive caudal fin in this paper, to investigate both the convergence to the straight line path, the achieved forward velocity, and the power consumption. Furthermore, comparison results for the USR with and without tail will be presented in Section 4.

The structure of the path following control approach is shown in Fig. 2. The control approach consists of a LOS guidance law responsible for producing the reference heading (orientation), the heading controller responsible for making the actual heading follow the desired one, and the gait pattern generator which produces the required undulatory motion to propel the robot forward. Note that for biologically inspired underwater snake robots, propulsion is commonly achieved by the interaction of the body with the surrounding water during body undulations. Hence, in this paper we use a general sinusoidal motion pattern introduced in Kelasidi et al. (2014), and make each joint $i \in \{1, \cdots, n-1\}$ of the robot follow the sinusoidal reference signal

$$\phi_i^*(t) = \alpha \mathrm{g}(i,n) \sin(\omega t + (i-1)\delta) + \phi_0, \tag{1}$$

where body undulations of constant amplitude (i.e. lateral undulation choosing $\mathrm{g}(i,n) = 1$) and increasing amplitude from the head to the tail (i.e. eel-like motion choosing $\mathrm{g}(i,n) = (n-i)/(n+1)$) can be achieved by a proper choice of the scaling function $\mathrm{g}(i,n)$. The maximum amplitude, the frequency and the phase shift between the joints of the sinusoidal motion pattern are denoted by α, ω and δ, respectively, while the phase offset ϕ_0 can be used to induce turning motion (Liljebäck et al., 2013; Guo, 2006). For the path following control approach, constant values are chosen for the parameters α, ω and δ, while the parameter ϕ_0 is used for directional control.

The control objective of the path following approach is to make the robot converge to the desired straight line path, with a nonzero forward velocity. Note that in this paper, we investigate only straight line path following for USRs. The desired path is aligned with the global x axis, and the actual heading of the robot is calculated as the average of the horizontal link angles as:

$$\theta = \frac{1}{n} \sum_{i=1}^{n} \theta_i. \tag{2}$$

In addition, the following LOS guidance law (Fossen, 2011) is used to define the desired heading θ_{ref} of the robot as a function of the position of the center of mass (CM) of the robot p_y along the global y axis (i.e. the cross track error):

$$\theta_{\mathrm{ref}} = -\arctan\left(\frac{p_y}{\Delta}\right), \qquad \Delta > 0 \tag{3}$$

where Δ is a design parameter referred as the *look-ahead distance* that influences the rate of convergence to the desired path and thus the transient motion of the robot (Fossen, 2011). See Kelasidi et al. (2016a) for more details.

As it is mentioned earlier the joint angle offset ϕ_0 is used for the directional control of the underwater snake robot. In this paper, the following simple P-controller is used to make the actual heading θ follow the desired one, θ_{ref}:

$$\phi_0 = k_\theta \left(\theta - \theta_{\mathrm{ref}}\right), \tag{4}$$

where $k_\theta > 0$ is a control gain (Kelasidi et al., 2016a).

4. EXPERIMENTAL STUDY

This section describes the experimental setup employed for the investigation of the path following control approach presented in Section 3. Furthermore, it presents experimental results using the straight line path following approach for Mamba with and without the passive caudal fin, and using both the lateral undulation and eel-like motion patterns.

4.1 Experimental Setup

The experiments were performed in a tank of dimensions L: 40 m, H: 1.5 m and W: 6.45 m in the MC-lab at NTNU (Marine cybernetics laboratory (MC-lab), 2016). The underwater camera positioning system consisting of six cameras from Qualisys (Qualisys–Motion Capture Systems, 2016), was used in order to obtain real time position and orientation measurements. In particular, it gave the position and orientation of an attachment at the last module consisting of five underwater reflective markers, as shown in Fig. 1b. The coverage area of the installed underwater camera system had dimensions 12 m$\times$1.35 m$\times$ 5.45 m, which were sufficient for the experimental trials presented in this paper. Note that the markers were submerged approximately 0.15 m in order to avoid reflections and thus provide accurate measurements, since the experiments were performed near the water surface. Afterwards, the obtained global frame measurements of the position and the orientation of the last module were combined with the measured joint angles in order to calculate the center of mass position and the link angles of the robot based on the kinematic equations. See Kelasidi et al. (2016a) for more details.

The illustration of the experimental setup is shown in Fig. 2. The path following approach presented in Section 3 was implemented on an external computer. The general sinusoidal motion pattern was calculated based on (1) and the reference joint angles were sent to each joint through the CAN bus. Note that during these experimental trials, a P-controller implemented in low level (i.e. in the microcontroller of each module) was responsible for making the joint angles follow the reference angles since the servos used in Mamba do not facilitate joint torque control.

The LOS path following control approach (2,3) was calculated with the look-ahead distance $\Delta = 0.18$ and the control gain $k_\theta = 0.4$ for all the experimental trials, as shown in Table 1, both for lateral undulation and the eel-like motion pattern. The gait parameters of the sinusoidal motion pattern were set to $\delta = 40^{\mathrm{o}}$ and $\omega = 90^{\mathrm{o}}/\mathrm{s}$ for both patterns, and $\alpha = 30^{\mathrm{o}}$ for lateral undulation and $\alpha = 40^{\mathrm{o}}$ for eel-like motion, respectively.

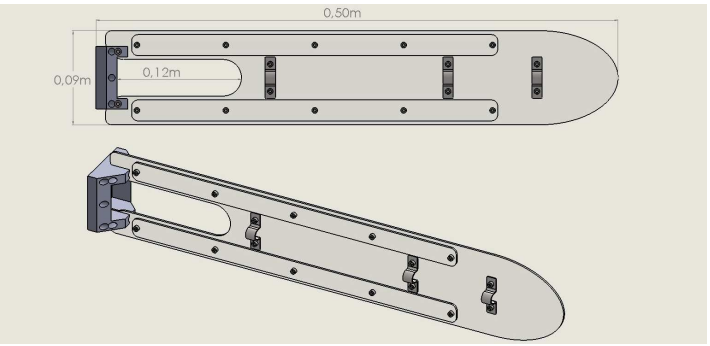

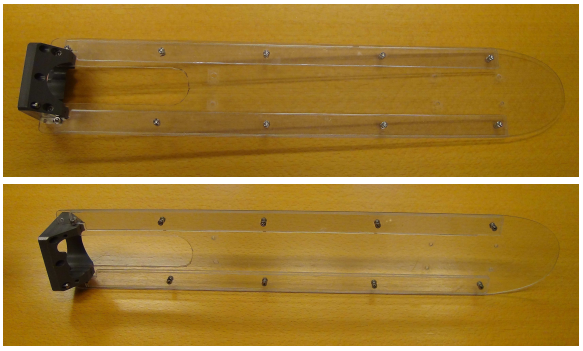

(a) Passive caudal (tail) fin

(b) Underwater snake robot Mamba with passive caudal fin attached at the last module of the robot

Fig. 1. Biologically inspired underwater snake robot with caudal fin.

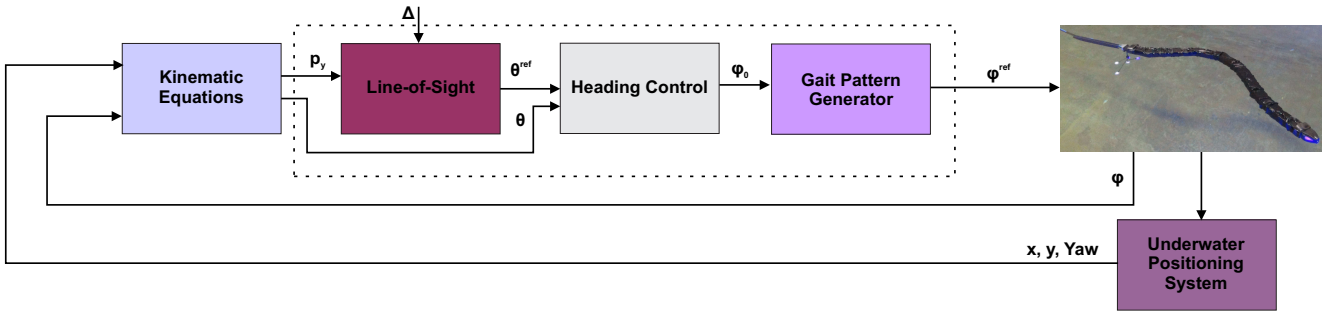

Fig. 2. Illustration of path following control approach for underwater snake robots.

Note that during the trials the joint offset $\phi_0 = [-20^o, 20^o]$ was saturated in order to consider the physical constraints of the joint angles of Mamba. In each trial the robot's joint angles were initially set to zero. The initial headings and the initial position of the center of mass of the robot are shown in Table 1 for each trial.

Furthermore, for the experimental trials presented in this paper the average power consumption was calculated using the following equation

$$P_{\text{avg}} = VI_{\text{avg}} - VI_0, \tag{5}$$

where $V = 35$ V and I_{avg} A is the average current obtained by using the multimeter FLUKE 289 which is able to provide measurements of the average, the maximum and the minimum values of the current. In particular, FLUKE 289 was attached to the power box that was connected to the power supply cable of Mamba during the experiments. An initial average current value of $I_0 = 1.18$ A was measured by the multimeter before applying the path following control approach, and was subtracted from the total average power consumption. Note that in this way we do not take into account the power consumed from the electronics inside the joint modules at rest, and thus we are able to provide more precise comparison results regarding the power consumption during the path following experimental trials.

Furthermore, the average forward velocity for each trial was calculated as

$$\bar{v}_t = \frac{\sqrt{(p_{\text{stop},x} - p_{\text{start},x})^2 + (p_{\text{stop},y} - p_{\text{start},y})^2}}{t_{\text{stop}} - t_{\text{start}}}, \tag{6}$$

where the positions $\mathbf{p}_{\text{start}}$ and $\mathbf{p}_{\text{stop}}$ denote the start and end points of the CM of the robot during the path following trials (i.e. the difference gives the traveled distance of the CM of the robot during the path following trials).

4.2 Experimental Results

In this section we compare the experimental results obtained using the USR Mamba with and without the passive caudal fin, for the two most common motion patterns for underwater snake robots: lateral undulation and eel-like motion pattern. For each trial, results were obtained for three different sets of initial positions and orientations of the robot. Comparison results for the average forward velocity and the average power consumption for all the different trials are shown in Table 1. Figures 3-5 and Figures 6-8 present the experimental results obtained using Mamba with and without the passive caudal fin, respectively, for the lateral undulation motion pattern. Similar results for the eel-like motion pattern from all the trials are shown in Figures 9-14.

As we can see from Figures 3a-14a, the robot managed to reach and follow the desired straight line path for all the trials with different initial conditions, both for the lateral undulation and eel-like motion patterns. In addition, it can be easily seen from Figures 3b-14b that the cross track error as expected converges towards and oscillates around zero, and from Figures 3c-14c that the heading controller managed to make the actual heading follow its reference for all the investigated cases. However, comparing Figures 3-5 with Figures 6-8 we can see that the convergence to the path was much faster for the case of Mamba with the passive caudal fin. In particular, the robot with the passive caudal fin managed to achieve almost double the forward speed (i.e. a 100 % increase in the forward velocity) compared to the robot without tail fin, as also seen in Table 1. Note that results presented in Kelasidi et al. (2015b) showed that by increasing the length of the robot by 100 % (i.e. increasing the number of the links from 10 links to 20 links) it is possible to increase the forward velocity by less than 20 %, both for lateral undulation and eel-like motion patterns. By attaching the passive tail fin, which results in a 30 % increase of the total length of the robot, we here see that we achieve an increase of 100 % in the forward velocity. At the same time, the results in Table 1 show that also the average power consumption is doubled when the tail fin is used. Similarly, a doubling of the number of links would also increase almost 10 times the average power consumption (Kelasidi et al., 2015b), but only result in less than 20% increase in the forward velocity. The experimental results thus indicate that the passive fin provides increased locomotion efficiency.

Another interesting observation is that the achieved forward velocity and the average power consumption are in the same order of magnitude for the different sets of initial positions in all the trials (Tables 1 and 2). Note that during each trial the gait parameters α, ω and δ were constant, as described in Section 4.1. In addition, in Kelasidi et al. (2015a) it was shown that the forward velocity and the power consumption are directly dependent on the gait parameters for the free swimming case (i.e. open loop control). Hence, we can conclude that the magnitude of the forward speed and the power consumption are independent on the initial conditions since we kept the same value for the gait parameters α, ω and δ, the look-ahead-distance Δ and the control gain K_θ in all the cases. This means that by choosing proper values of these parameters we can do open-loop control of the forward velocity and the power consumption, which is in accordance with the theoretical results obtained based on averaging theory, and the simulation and experimental results that are presented in Kelasidi et al. (2015a). The experimental results in this paper furthermore indicate that the properties derived and experimentally validated in Kelasidi et al. (2015a) for an underwater snake robot without caudal fin, also hold when we close the loop (i.e. path following control).

Table 1. Comparison results for USR with and without passive caudal fin.

	Δ [m]	K_θ	θ_0 [deg]	$\bar{v}_t$ [m/s]	P_{avg} [W]
Lateral Undulation without passive caudal fin					
Case 1	0.18	0.4	-1.86 ^{o}	0.0936	51.7860
Case 2	0.18	0.4	-28.8400	0.0892	50.1095
Case 3	0.18	0.4	49.46	0.0883	50.3300
Lateral Undulation with passive caudal fin					
Case 1	0.18	0.4	7.7^o	0.1938	97.8985
Case 2	0.18	0.4	-19.06	0.1983	98.5950
Case 3	0.18	0.4	41.49	0.1848	99.2950
Eel-like motion without passive caudal fin					
Case 1	0.18	0.4	-1.94	0.0878	50.0185
Case 2	0.18	0.4	-24.96	0.0925	50.3825
Case 3	0.18	0.4	36.66	0.0846	51.4850
Eel-like motion with passive caudal fin					
Case 1	0.18	0.4	-2.76	0.1773	99.5050
Case 2	0.18	0.4	-24.73	0.1724	98.0000
Case 3	0.18	0.4	49.51	0.1510	96.9850

5. CONCLUSIONS AND FUTURE WORK

In this paper experimental results have been presented for path following control of the bioinpired underwater snake robot Mamba, comparing its performance with and without a passive caudal fin. In particular, it was shown that a path following approach previously proposed for underwater snake robots without tail fin, can be applied to solve the path following control problem of the USR with caudal fin without any modification. In particular, it was shown that the path following control approach successfully steers the robot towards and along the desired path. Comparison experimental results were presented for the most common motion patterns for USRs, the lateral undulation and the eel-like motion pattern. Based on this comparison, a main advantage of equipping the underwater snake robot with a passive tail fin compared to the configuration without any external effectors presented in Kelasidi et al. (2016a), and the configuration of the robot with a tail thruster module presented in Kelasidi et al. (2016b), is that by simply attaching a passive caudal fin it is possible to increase the forward velocity 100 % with a relatively low increase in power consumption, and with a minimum increase in the complexity of the mechanical design.

In future work, we will investigate the locomotion efficiency of USRs with an active caudal fin. Comparison results regarding the locomotion efficiency with and without passive/active caudal fins for underwater snake robots will bring new insights for the development of the next generation of bioinspired underwater snake robots.

ACKNOWLEDGEMENTS

The authors gratefully acknowledge the engineers at the Department of Engineering Cybernetics, Terje Haugen, Glenn Angell and Daniel Bogen, for implementing the necessary components for the experimental setup and the PhD student Signe Moe for her contribution on obtaining the experimental results.

REFERENCES

Alamir, M., El Rafei, M., Hafidi, G., Marchand, N., Porez, M., and Boyer, F. (2007). Feedback design for 3D movement of

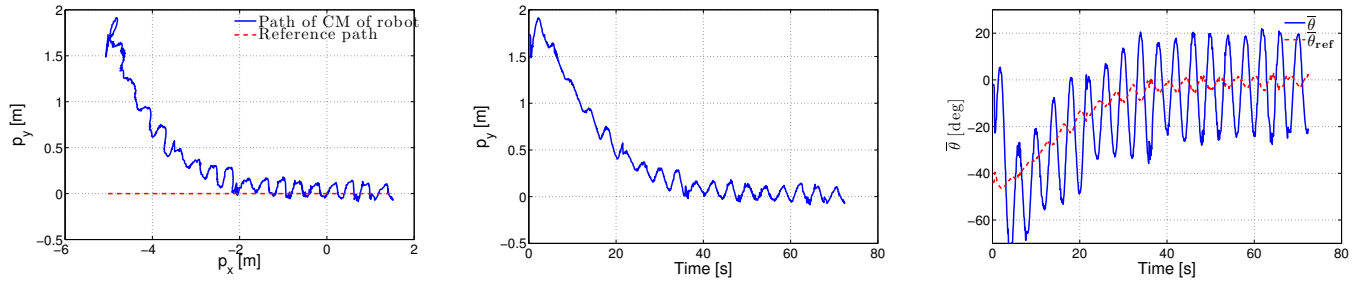

(a) Path of the CM (blue) and the reference path (red)

(b) Cross track error, p_y

(c) Heading angle, $\overline{\theta}$ (blue) and the reference heading angle, $\overline{\theta}_{\text{ref}}$ (red)

Fig. 3. Case 1 for lateral undulation: Straight line path following with the physical snake without tail fin with the initial distance from the CM being $p_y = 1.7352$ m.

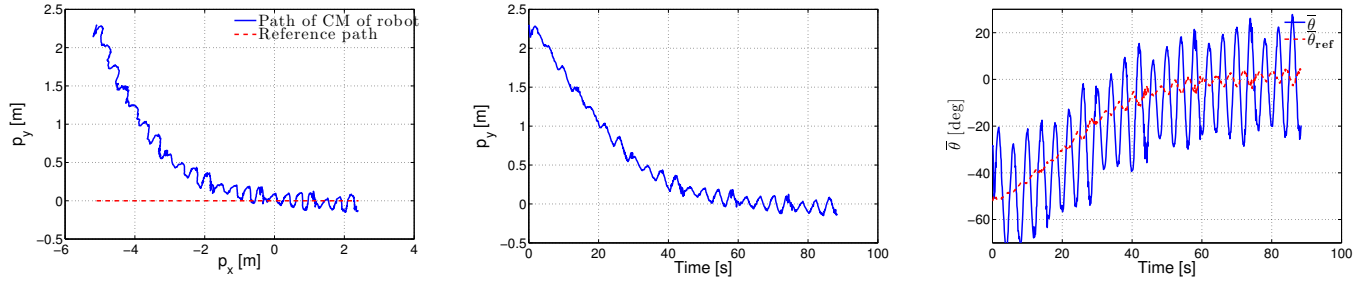

(a) Path of the CM (blue) and the reference path (red)

(b) Cross track error, p_y

(c) Heading angle, $\overline{\theta}$ (blue) and the reference heading angle, $\overline{\theta}_{\text{ref}}$ (red)

Fig. 4. Case 2 for lateral undulation: Straight line path following with the physical snake without tail fin with the initial distance from the CM being $p_y = 2.2867$ m.

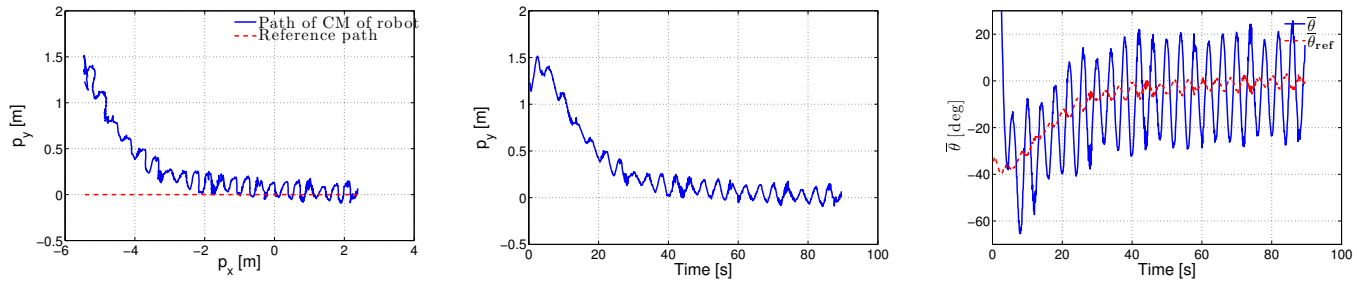

(a) Path of the CM (blue) and the reference path (red)

(b) Cross track error, p_y

(c) Heading angle, $\overline{\theta}$ (blue) and the reference heading angle, $\overline{\theta}_{\text{ref}}$ (red)

Fig. 5. Case 3 for lateral undulation: Straight line path following with the physical snake without tail fin with the initial distance from the CM being $p_y = 1.2235$ m.

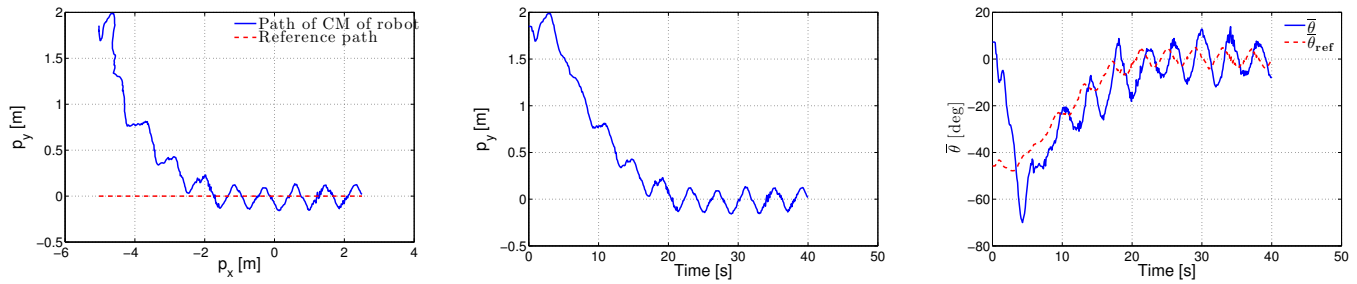

(a) Path of the CM (blue) and the reference path (red)

(b) Cross track error, p_y

(c) Heading angle, $\overline{\theta}$ (blue) and the reference heading angle, $\overline{\theta}_{\text{ref}}$ (red)

Fig. 6. Case 1 for lateral undulation: Straight line path following with the physical snake with tail fin with the initial distance from the CM being $p_y = 1.848$ m.

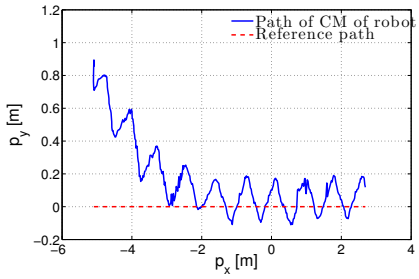

(a) Path of the CM (blue) and the reference path (red)

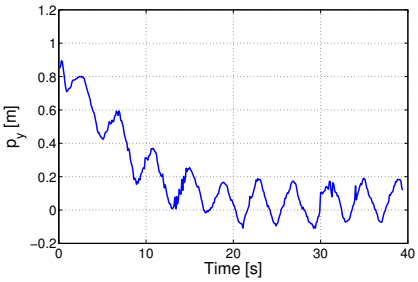

(b) Cross track error, p_y

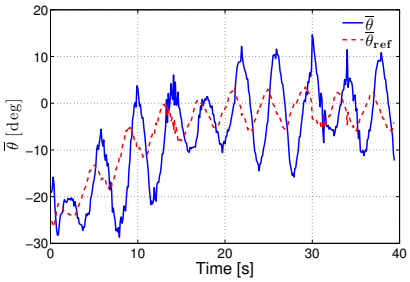

(c) Heading angle, $\overline{\theta}$ (blue) and the reference heading angle, $\overline{\theta}_{\text{ref}}$ (red)

Fig. 7. Case 2 for lateral undulation: Straight line path following with the physical snake with tail fin with the initial distance from the CM being $p_y = 0.8515$ m.

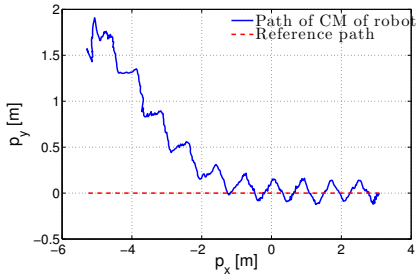

(a) Path of the CM (blue) and the reference path (red)

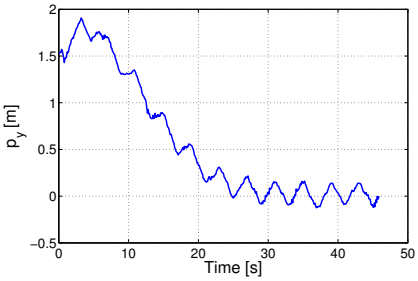

(b) Cross track error, p_y

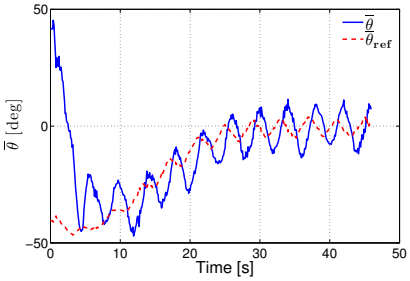

(c) Heading angle, $\overline{\theta}$ (blue) and the reference heading angle, $\overline{\theta}_{\text{ref}}$ (red)

Fig. 8. Case 3 for lateral undulation: Straight line path following with the physical snake with tail fin with the initial distance from the CM being $p_y = 1.5344$ m.

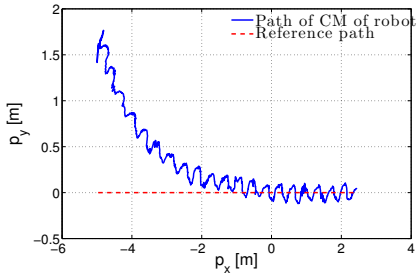

(a) Path of the CM (blue) and the reference path (red)

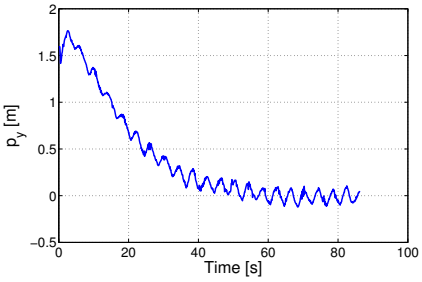

(b) Cross track error, p_y

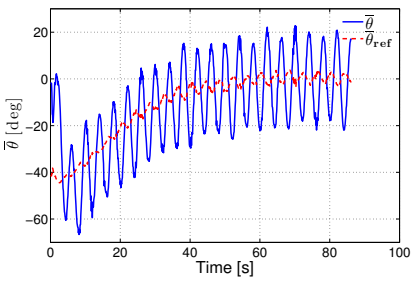

(c) Heading angle, $\overline{\theta}$ (blue) and the reference heading angle, $\overline{\theta}_{\text{ref}}$ (red)

Fig. 9. Case 1 for eel-like motion pattern: Straight line path following with the physical snake without tail fin with the initial distance from the CM being $p_y = 1.5932$ m.

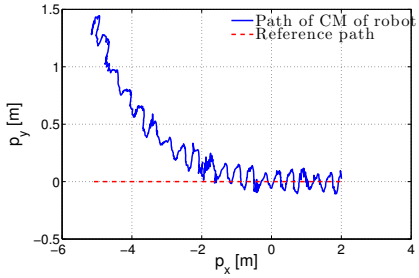

(a) Path of the CM (blue) and the reference path (red)

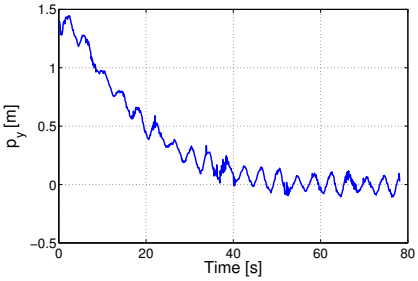

(b) Cross track error, p_y

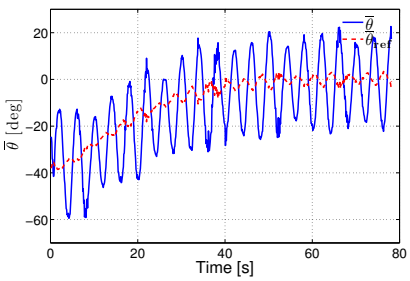

(c) Heading angle, $\overline{\theta}$ (blue) and the reference heading angle, $\overline{\theta}_{\text{ref}}$ (red)

Fig. 10. Case 2 for eel-like motion pattern: Straight line path following with the physical snake without tail fin with the initial distance from the CM being $p_y = 1.3950$ m.

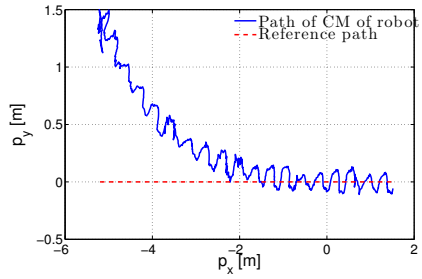

(a) Path of the CM (blue) and the reference path (red)

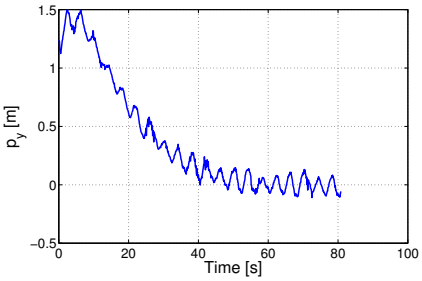

(b) Cross track error, p_y

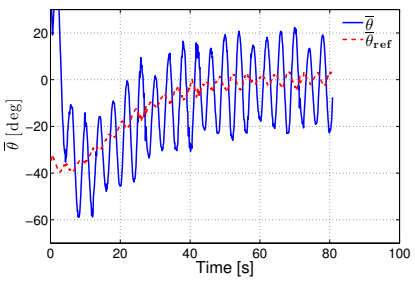

(c) Heading angle, $\overline{\theta}$ (blue) and the reference heading angle, $\overline{\theta}_{\text{ref}}$ (red)

Fig. 11. Case 3 for eel-like motion pattern: Straight line path following with the physical snake without tail fin with the initial distance from the CM being $p_y = 1.2312$ m.

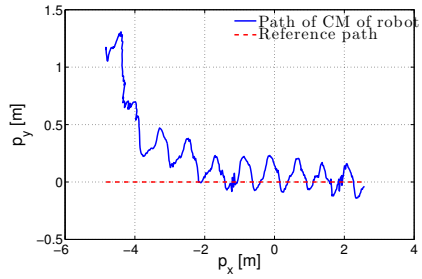

(a) Path of the CM (blue) and the reference path (red)

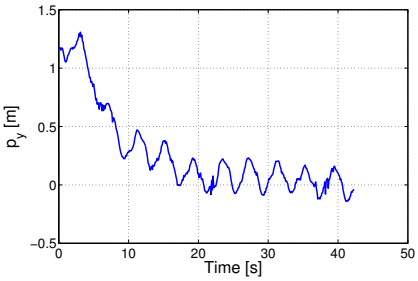

(b) Cross track error, p_y

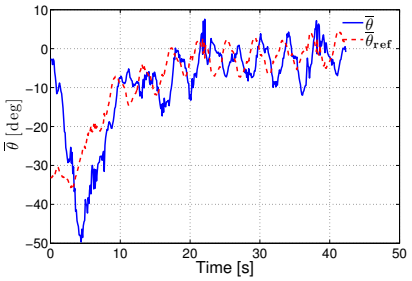

(c) Heading angle, $\overline{\theta}$ (blue) and the reference heading angle, $\overline{\theta}_{\text{ref}}$ (red)

Fig. 12. Case 1 for eel-like motion pattern: Straight line path following with the physical snake with tail fin with the initial distance from the CM being $p_y = 1.1758$ m.

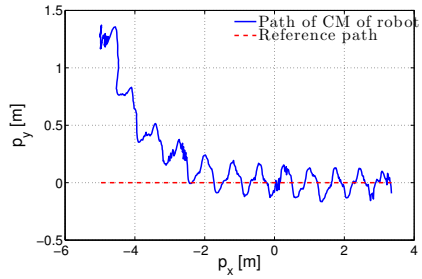

(a) Path of the CM (blue) and the reference path (red)

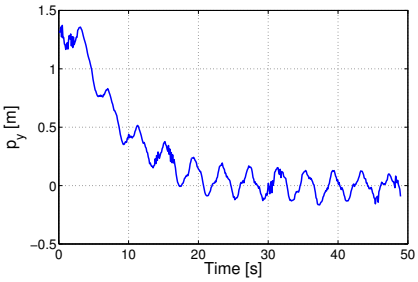

(b) Cross track error, p_y

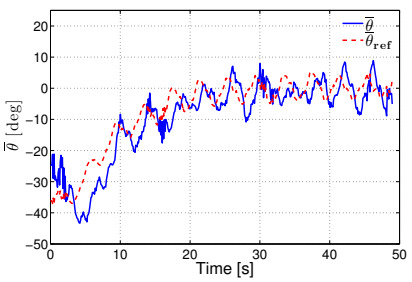

(c) Heading angle, $\overline{\theta}$ (blue) and the reference heading angle, $\overline{\theta}_{\text{ref}}$ (red)

Fig. 13. Case 2 for eel-like motion pattern: Straight line path following with the physical snake with tail fin with the initial distance from the CM being $p_y = 1.3134$ m.

an eel-like robot. In *Proc. IEEE International Conference on Robotics and Automation (ICRA)*, 256–261. Roma.

Ayers, J., Wilbur, C., and Olcott, C. (2000). Lamprey robots. In *Proc. International Symposium on Aqua Biomechanisms*.

Crespi, A. and Ijspeert, A.J. (2006). AmphiBot II: An Amphibious Snake Robot that Crawls and Swims using a Central Pattern Generator. In *Proc. 9th International Conference on Climbing and Walking Robots (CLAWAR)*, 19–27. Brussels, Belgium.

Crespi, R., Badertscher, A., Guignard, A., and Ijspeert, A.J. (2005). Amphibot I: an amphibious snake-like robot. *Robotics and Autonomous Systems*, 50(4), 163–175.

Fossen, T.I. (2011). *Handbook of Marine Craft Hydrodynamics and Motion Control*. John Wiley & Sons, Ltd.

Guo, J. (2006). A waypoint-tracking controller for a biomimetic autonomous underwater vehicle. *Ocean Engineering*, 33(17-18), 2369 – 2380.

Kelasidi, E., Liljebäck, P., Pettersen, K.Y., and Gravdahl, J.T. (2015a). Experimental investigation of efficient locomotion of underwater snake robots for lateral undulation and eel-like motion patterns. *Robotics and Biomimetics*, 2(1), 1–27.

Kelasidi, E., Liljebäck, P., Pettersen, K.Y., and Gravdahl, J.T. (2016a). Innovation in underwater robots: Biologically inspired swimming snake robots. *IEEE Robotics Automation Magazine*, 23(1), 44–62.

Kelasidi, E., Liljebäck, P., Pettersen, K.Y., and Gravdahl, J.T. (2017). Integral line-of-sight guidance for path following control of underwater snake robots: Theory

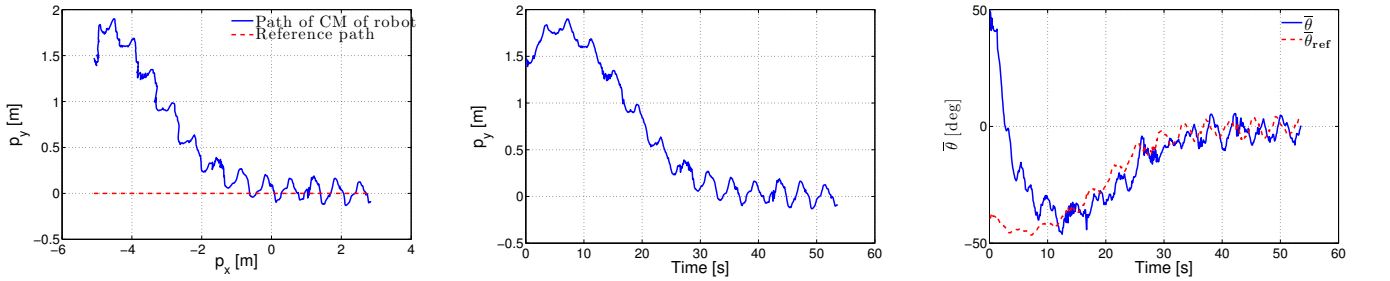

(a) Path of the CM (blue) and the reference path (red)

(b) Cross track error, p_y

(c) Heading angle, $\overline{\theta}$ (blue) and the reference heading angle, $\overline{\theta}_{\text{ref}}$ (red)

Fig. 14. Case 3 for eel-like motion pattern: Straight line path following with the physical snake with tail fin with the initial distance from the CM being $p_y = 1.4722$ m.

and experiments. *IEEE Transactions on Robotics*, PP(99), 1–19. doi:10.1109/TRO.2017.2651119. DOI:10.1109/TRO.2017.2651119.

Kelasidi, E., Pettersen, K.Y., and Gravdahl, J.T. (2015b). Energy efficiency of underwater snake robot locomotion. In *Proc. 23th Mediterranean Conference on Control Automation (MED)*. Torremolinos, Spain.

Kelasidi, E., Pettersen, K.Y., Liljebäck, P., and Gravdahl, J.T. (2014). Integral line-of-sight for path-following of underwater snake robots. In *Proc. IEEE Multi-Conference on Systems and Control*, 1078 – 1085. Antibes, France.

Kelasidi, E., Pettersen, K.Y., Liljebck, P., and Gravdahl, J.T. (2016b). Locomotion efficiency of underwater snake robots with thrusters. In *Proc. IEEE International Symposium on Safety, Security, and Rescue Robotics (SSRR)*, 174–181. Lausanne, Switzerland.

Knutsen, T., Ostrowski, J., and McIsaac, K. (2004). Designing an underwater eel-like robot and developing anguilliform locomotion control. *NSF Summer Undergraduate Fellowship in Sensor Technologies, Tamara Harvard University*, 119–142.

Kruusmaa, M., Fiorini, P., Megill, W., De Vittorio, M., Akanyeti, O., Visentin, F., Chambers, L., El Daou, H., Fiazza, M.C., Jezov, J., Listak, M., Rossi, L., Salumae, T., Toming, G., Venturelli, R., Jung, D., Brown, J., Rizzi, F., Qualtieri, A., Maud, J., and Liszewski, A. (2014). Filose for svenning: A flow sensing bioinspired robot. *IEEE Robotics Automation Magazine*, 21(3), 51–62.

Lapierre, L. and Jouvencel, B. (2005). Path following control for an eel-like robot. In *Proc. MTS/IEEE International Conference Oceans*, 460–465. Brest, France.

Li, B., Yu, S., Ma, S., and Wang, Y. (2011). An amphibious snake-like robot with novel gaits on ground and in water. In *Proc. IASTED International Conference Intelligent Systems and Control (ISC 2011)*, 100–105. Calgary, AB.

Liljebäck, P., Pettersen, K.Y., Stavdahl, Ø., and Gravdahl, J.T. (2013). *Snake Robots: Modelling, Mechatronics, and Control*. Springer-Verlag, Advances in Industrial Control.

Liljebäck, P., Stavdahl, Ø., Pettersen, K., and Gravdahl, J. (2014). Mamba - a waterproof snake robot with tactile sensing. In *Proc. International Conference on Intelligent Robots and Systems (IROS)*, 294–301. Chicago, IL.

Marine cybernetics laboratory (MC-lab) (2016). URL `http://www.ntnu.no/imt/lab/cybernetics`.

McIsaac, K. and Ostrowski, J. (2002). Experiments in closed-loop control for an underwater eel-like robot. In *Proc. IEEE International Conference on Robotics and Automation (ICRA)*, 750–755. Washington DC.

McIsaac, K. and Ostrowski, J. (2003). Motion planning for anguilliform locomotion. *IEEE Transactions on Robotics and Automation*, 19(4), 637–625.

Mclsaac, K. and Ostrowski, J. (1999). A geometric approach to anguilliform locomotion: modelling of an underwater eel robot. In *Proc. International Conference on Robotics and Automation (ICRA)*, volume 4, 2843–2848. Detroit, MI.

Porez, M., Boyer, F., and Ijspeert, A.J. (2014). Improved lighthill fish swimming model for bio-inspired robots: Modeling, computational aspects and experimental comparisons. *The International Journal of Robotics Research*, 33(10), 1322–1341.

Qualisys–Motion Capture Systems (2016). URL `http://www.qualisys.com`.

Stefanini, C., Orofino, S., Manfredi, L., Mintchev, S., Marrazza, S., Assaf, T., Capantini, L., Sinibaldi, E., Grillner, S., Wallen, P., and Dario, P. (2012). A novel autonomous, bioinspired swimming robot developed by neuroscientists and bioengineers. *Bioinspiration & Biomimetics*, 7(2), 025001.

Sverdrup-Thygeson, J., Kelasidi, E., Pettersen, K.Y., and Gravdahl, J.T. (2016a). A control framework for biologically inspired underwater swimming manipulators equipped with thrusters. In *Proc.10th IFAC Conference on Control Applications in Marine Systems (CAMS)*. Trondheim, Norway.

Sverdrup-Thygeson, J., Kelasidi, E., Pettersen, K.Y., and Gravdahl, J.T. (2016b). Modeling of underwater swimming manipulators. In *Proc.10th IFAC Conference on Control Applications in Marine Systems (CAMS)*. Trondheim, Norway.

Takayama, T. and Hirose, S. (2002). Amphibious 3d active cord mechanism "helix" with helical swimming motion. In *Proc. IEEE/RSJ International Conference on Intelligent Robots and Systems (IROS)*, volume 1, 775 – 780. Lausanne, Switzerland.

Wilbur, C., Vorus, W., Cao, Y., and Currie, S. (2002). *Neurotechnology for biomimetic robots, chapter A Lamprey-Based Undulatory Vehicle*. Bradford/MIT Press.

Yamada, H., Chigisaki, S., Mori, M., Takita, K., Ogami, K., and Hirose, S. (2005). Development of amphibious snake-like robot ACM-R5. In *Proc. 36th International Symposium on Robotics*. Tokyo, Japan.

Ye, C., Ma, S., Li, B., and Wang, Y. (2004). Locomotion control of a novel snake-like robot. In *Proc. IEEE/RSJ International Conference on Intelligent Robots and Systems (IROS)*, 925–930. Sendai, Japan.